

Article

Estimating Soil Hydraulic Parameters during Ponding Infiltration Using a Hybrid Algorithm

Yibo Li ¹, Ye Liu ^{2,3} and Xiaoyi Ma ^{2,3,*}

¹ State Key Laboratory of Eco-Hydraulics in Northwest Arid Region, Xi'an University of Technology, Xi'an 710048, China

² College of Water Resources and Architectural Engineering, Northwest A&F University, Xianyang 712100, China

³ Key Laboratory of Agricultural Soil and Water Engineering in Arid and Semiarid Areas, Ministry of Education, Northwest A&F University, Xianyang 712100, China

* Correspondence: xma@nwafu.edu.cn

Abstract: Accurate inversion of soil hydraulic parameters based on the van Genuchten–Mualem model has received much attention in soil science research. Herein, a hybrid algorithm method using particle swarm optimization and vector-evaluated genetic algorithm was used to invert the parameters θ_s , α , n , and K_s , with the objective functions of infiltration rate, cumulative infiltration, and soil water content. Then, numerical experiments were conducted on four typical soils at three initial water content levels (20, 40, and 60% effective saturation) to verify the accuracy of the inverse method. The results showed that the inversed soil water retention and conductivity curves were approximately the same as the real curves, with the root mean square errors of $0.00101\text{--}0.00192\text{ cm}^3\cdot\text{cm}^{-3}$, $0.00800\text{--}0.02519\text{ cm}^3\cdot\text{cm}^{-3}$, respectively, and both the Nash–Sutcliffe coefficients were approximately 1.0. Additionally, laboratory experiments were also performed to compare with the inversed parameters for verification, within small root mean squared errors and approximately 1.0 Nash–Sutcliffe coefficients. Furthermore, the method can also achieve acceptably accurate parameter inversion even with substantial measurement errors included in the cumulative infiltration, initial water content, and final water content. Thus, the method is effective and robust and found to be practical in field experiments.

Keywords: parameter estimation; soil hydraulic properties; inverse modeling; vector-evaluated genetic algorithm; SWMS-2D



Citation: Li, Y.; Liu, Y.; Ma, X.

Estimating Soil Hydraulic Parameters during Ponding Infiltration Using a Hybrid Algorithm. *Agronomy* **2023**, *13*, 726. <https://doi.org/10.3390/agronomy13030726>

Academic Editors: Xuguang Xing, Ankit Garg and Long Zhao

Received: 29 December 2022

Revised: 22 February 2023

Accepted: 25 February 2023

Published: 28 February 2023



Copyright: © 2023 by the authors. Licensee MDPI, Basel, Switzerland. This article is an open access article distributed under the terms and conditions of the Creative Commons Attribution (CC BY) license (<https://creativecommons.org/licenses/by/4.0/>).

1. Introduction

Numerical models describing the flow and transport of water and chemicals through the vadose zone have been increasingly and extensively applied in field-scale research. When these models are used to simulate saturated water flow and contaminant transport, it is critical to have a good understanding of unsaturated soil hydraulic properties, as the outcome from applying these models depends on the accuracy of model evaluation. Unsaturated hydraulic conductivity, $K(\theta)$ and soil water retention, $h(\theta)$ are often required to solve the Richards equation numerically. However, the extreme spatial heterogeneity of a subsurface environment confounds measurement of these hydraulic properties [1,2]. Hydraulic properties may exhibit significant variation over time due to changes in the ionic composition and concentration of a soil solution, the impact of soil crust and particle dispersion, shrink-swell phenomena in fine-textured soil, and cultivation or other agricultural activities [3].

The soil water diffusivity, D , and hydraulic conductivity, K , can be measured directly by laboratory and field methods as a function of water content or pressure head [4,5]. Direct measurement methods are relatively simple in concept, but several limitations restrict their practical usage [6]. As a result, the application of direct measurement methods in field gravity drainage experiments of layered profiles, or medium- and fine-textured soils is limited. In addition, methods that require equilibrium conditions, such as repeated steady-state flow situations, are time-consuming. Additionally, additional errors are introduced

by approximation or interpolation, including linearization to facilitate semi-analytic or analytic inversion of the flow equation. Lastly, direct inversion methods cannot be used to obtain information about uncertainty in the estimated hydraulic parameters by means of closed analytical equations, but to determine them by iterative solution methods, which also places high demands on computational resources [7].

Parameter optimization methods present a more flexible way to solve the inverse problems [8,9]. With the rapid development of computer science, machine learning and optimization algorithms have been widely used in a variety of fields such as machine design [10,11], image identification [12–14], and data analysis and mining [15,16], providing additional opportunities for parameter optimization. Optimization procedures facilitate simultaneous estimation of hydraulic and retention conductivity functions based on transient flow data [17]. Previous parameter optimization studies mainly concentrated on solute transport [18,19]. It was first described by Dane and Hruska [20] and Zachmann [21]. Parameter estimation has been increasingly used to estimate hydraulic functions of unsaturated soil. Parker [22] and Kool [23,24] developed computational models for one-step laboratory column outflow measurements, whereas Eching and Hopmans [25] and van Dam [26] developed computational models for multi-step laboratory column measurements. During ponded infiltration experiments, the estimation of soil hydraulic properties has also received considerable attention [27,28]. At first, inverse methods were mostly applied to laboratory-type experiments, but they are equally suitable for applications to field data [29] and a proper combination of laboratory and field data. Inverse procedures have a significant advantage that researchers can perform a relatively easy detailed error analysis of the estimated parameters in the context of a parameter optimization problem [7,30]. Although parameter optimization methods have several advantages, there are still some problems related to parameter uniqueness, convergence, and computational efficiency, especially at the time of simultaneous estimation of numerous hydraulic parameters [31].

Previously, a novel two-step inverse approach was proposed based on a particle swarm optimization (PSO) and vector-evaluated genetic algorithm (VEGA) with negative hydraulic head [32]. However, considering the actual situation that most irrigation activities in agriculture are the positive water depth, this study focuses on numerical inversion of soil hydraulic parameters for ponding infiltration, with practical significance. In addition, with the introduction of new formulations of α/K_s and v/K_s , the efficiency of the inverse procedure was shown to be improved in this study. Furthermore, laboratory experiments with three different levels of soil water conductivity were carried out to compare with the simulated values for verification. An overview of the research flow is shown in Figure 1. In the following sections, the theoretical foundations and the inverse procedures are described. This is followed by the numerical and laboratory experiments, the validation of the models, as well as the precision analysis.

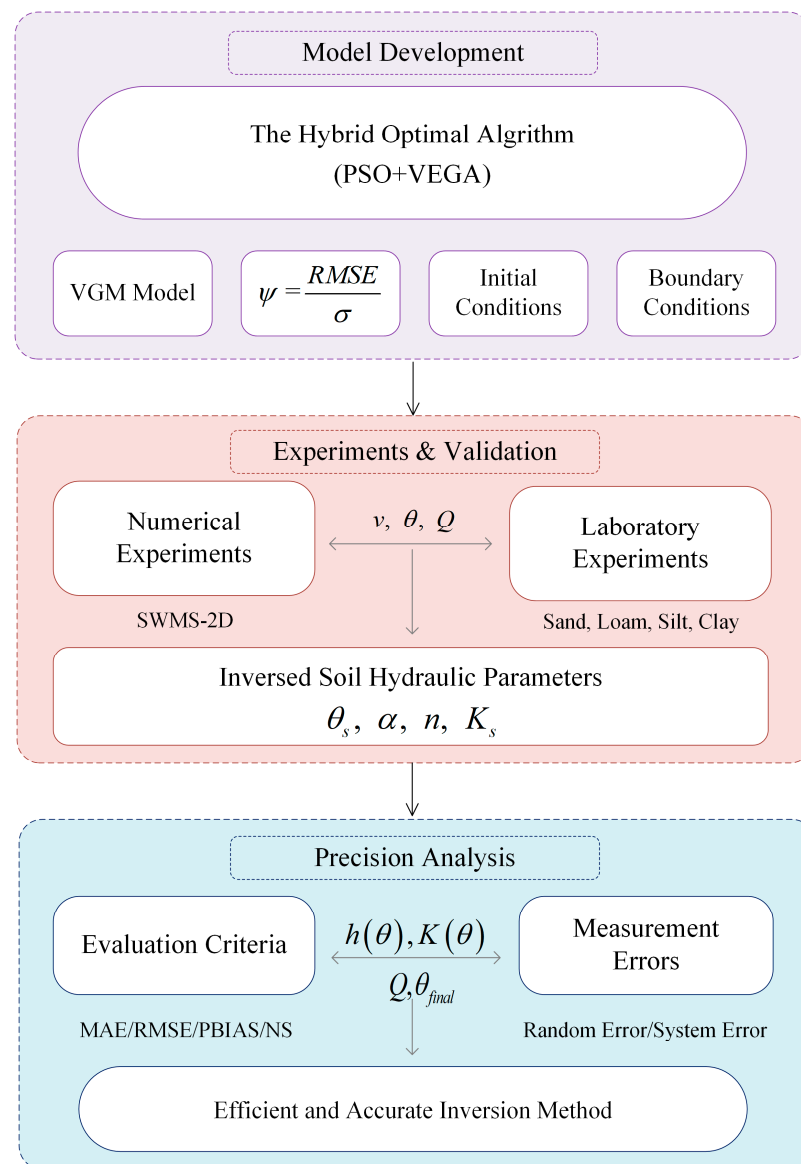


Figure 1. A flowchart overview of the research process.

2. Theoretical Foundation

2.1. Water Flow

Assuming that the air phase plays a non-significant role in the liquid flow process, the flow equation governing radially symmetric isothermal Darcy flow in a variably porous, rigid, isotropic, and saturated medium is given by the modified form of the Richards equation as follows:

$$\frac{\partial \theta}{\partial t} = \frac{\partial}{\partial r} \left[K(h) \frac{\partial h}{\partial r} \right] + \frac{K(h)}{r} \frac{\partial h}{\partial r} + \frac{\partial}{\partial z} \left[K(h) \left(\frac{\partial h}{\partial z} - 1 \right) \right] \quad (1)$$

where t is time (min); r is the radial coordinate (cm); z is the depth of soil surface (cm) with a positive value indicating a downward direction; $K(h)$ is the hydraulic conductivity ($\text{cm} \cdot \text{min}^{-1}$); h is the potential head (cm), and θ is the soil water content ($\text{cm}^3 \cdot \text{cm}^{-3}$).

In Equation (1), the root water uptake by plant roots was not considered and the porous medium was assumed to be isotropic. Additionally, it was also assumed that the metric

head (h_i) and initial water content (θ_i) were the same in the vertical direction. Equation (1) was solved numerically, followed by the initial and boundary equations (Equations (2)–(5)):

$$\theta(r, z, t) = \theta_i, t = 0 \quad (2)$$

$$h(r, z, t) = h_i, t = 0 \quad (3)$$

$$h(r, z, t) = h_0(t), 0 < r < r_0, z = 0 \quad (4)$$

$$-\frac{\partial h(r, z, t)}{\partial z} - 1 = 0, r > r_0, z = 0 \quad (5)$$

$$h(r, z, t) = h_i, r^2 + z^2 \rightarrow \infty \quad (6)$$

where r_0 is the disc radius; h_0 is the time-variable supply pressure head, and h_i is the initial pressure head. The SWMS [33] was used to solve Equation (1) under the previously mentioned initial and boundary conditions. Van Genuchten [31] proposed a mass-conservative iterative scheme on which the numerical solution was based.

2.2. Soil Hydraulic Properties

Prior to the numerical solution of the Richards equation, a parametric model of unsaturated soil hydraulic properties was selected by the parameter optimization approach. In this study, the unsaturated soil hydraulic functions of the van Genuchten–Mualem model [34] was adopted to describe the soil water conductivity curve (SWCC) and soil water retention curve (SWRC):

$$S_e = \frac{\theta - \theta_r}{\theta_s - \theta_r} = \frac{1}{(1 + |\alpha h|^n)^m}, \quad (7)$$

$$K(\theta) = K_s S_e^l \left[1 - (1 - S_e^{\frac{1}{m}})^m \right]^2, \quad (8)$$

where $m = 1 - 1/n$; K_s is the saturated hydraulic conductivity ($\text{cm} \cdot \text{min}^{-1}$); l is an empirical shape parameter equal to 0.5; n is an empirical parameter associated with the pore-size distribution; α is an empirical parameter inversely associated with the air-entry pressure (cm^{-1}); θ_r is the residual water content level ($\text{cm}^3 \cdot \text{cm}^{-3}$); θ_s is the saturated water content level ($\text{cm}^3 \cdot \text{cm}^{-3}$); S_e is the effective saturation.

3. Inverse Procedure

3.1. Inverse Problem and Hybrid Optimal Algorithm

As shown in Equations (7) and (8), $h(\theta)$ and $K(\theta)$ are highly related to the effective saturation, S_e . Equation (7) demonstrates that the parameters θ_r and θ_s have a collinear relationship that cannot be inverted simultaneously. Moreover, θ_r is relatively small and can be obtained through the application of a transfer function to other physical soil characteristics [35–37]. Hence, the value of θ_r is set as the true value in the following inverse procedure. In the van Genuchten–Mualem model, the three parameters α , n , and K_s exhibit a complex nonlinear relationship, especially the parameters α and K_s which have a wide range of the order of magnitude, making it harder to be used in an inverse model.

During the infiltration process, potential head (h), infiltration rate (v), cumulative infiltration (Q), and soil water content (θ) can be used to estimate soil hydraulic parameters, but it is difficult to measure h . Thus, soil hydraulic parameters can be inverted based on θ , Q , and v in this study. Table 1 displays the soil hydraulic parameters of 12 typical soils obtained from RETC. Figure 2 details three kinds of parameter-pair relationships: α - K_s (a), α - n (b), and v - K_s (c). Figure 2a demonstrates that with the increase of α , the corresponding n increases linearly and K_s increases sharply. Thus, it is necessary to consider correlations between these parameters in future research; otherwise, analysis of physical mechanisms is unreasonable and difficult to perform in the inverse model. Therefore, the ratio of α/K_s

can be used in the inverse model. To improve the presentation of the inverse work, a comprehensive summary of the scopes of soil hydraulic parameters (K_s , n , α , θ_s , and θ_r) and the ratio of α/K_s were mostly taken from the Unsaturated Soil Database (UNSODA) [38], as well as from a further 192 published available literatures, as shown in Table 2, covering the majority of soil conditions.

Table 1. Soil hydraulic parameters for the van Genuchten–Mualem model (RETc).

Texture Class	θ_r $\text{cm}^3 \cdot \text{cm}^{-3}$	θ_s $\text{cm}^3 \cdot \text{cm}^{-3}$	α cm^{-1}	n -	l -	K_s $\text{cm} \cdot \text{min}^{-1}$	α/K_s
Sand	0.045	0.43	0.145	2.68	0.5	0.49500	0.293
Loamy sand	0.057	0.41	0.124	2.28	0.5	0.24317	0.510
Sandy loam	0.065	0.41	0.075	1.89	0.5	0.07367	1.018
Loam	0.078	0.43	0.036	1.56	0.5	0.01733	2.077
Silt	0.034	0.46	0.016	1.37	0.5	0.00417	3.840
Silt loam	0.067	0.45	0.020	1.41	0.5	0.00750	2.667
Sandy clay loam	0.100	0.39	0.059	1.48	0.5	0.02183	2.702
Clay loam	0.095	0.41	0.019	1.31	0.5	0.00433	4.385
Silty clay loam	0.089	0.43	0.010	1.23	0.5	0.00117	8.571
Sandy clay	0.100	0.38	0.027	1.23	0.5	0.00200	13.500
Silty clay	0.070	0.36	0.005	1.09	0.5	0.00033	15.000
Clay	0.068	0.38	0.008	1.09	0.5	0.00333	2.400

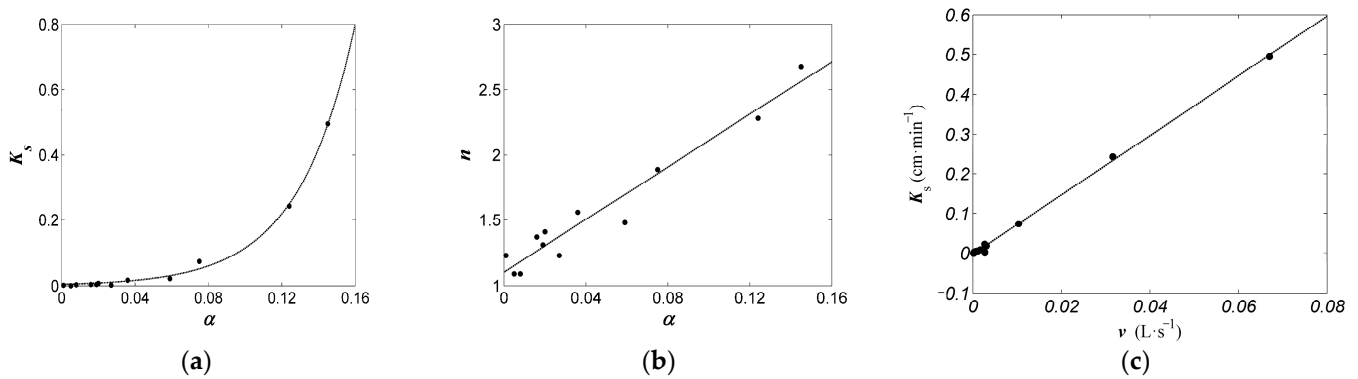


Figure 2. Relationships between selected soil hydraulic parameters: (a) α - K_s ; (b) α - n , and (c) v - K_s .

Table 2. Inverse scope of soil hydraulic parameters.

Scope	θ_s -	α cm^{-1}	n -	l -	K_s $\text{cm} \cdot \text{min}^{-1}$	α/K_s -	v/K_s -
minimum	0.35	0.001	1.05	0.5	0.00010	0.2	2
maximum	0.55	0.200	3.00	0.5	0.60000	20	60

A correct and relatively small range of parameters is critical for determining optimal values. Even when a restrictive range of α/K_s is employed, the range of K_s remains relatively large (6000 times of difference in magnitude), which is difficult to use in an optimal algorithm. During the infiltration process, the saturated conductivity (K_s) strongly influences the infiltration rate (v). The relationship between K_s and v for 12 typical soils with three depths (2, 3, and 5 cm) of ponding water is illustrated in Figure 2c. The infiltration rate was obtained using SWMS-2D, for which cumulative infiltration was simulated every 5 min. All the datasets were found to range from approximately 2 to 60, providing a narrow range (30 times), compared with the original range of K_s for the inverse algorithm. Hence, the ranges of both α/K_s and v/K_s were employed in the inverse procedure.

During the parameter inversion process, the objective function ψ is minimized and used to structure a response surface. The function can be expressed by one or a combination of θ , v , and Q . Most relevant studies have formulated objective functions to estimate

parameters using various combinations of θ , v , and Q , which can be used to transform into a single-objective optimization problem from a multi-objective optimization problem. However, it is difficult to determine a reasonable weight for the combination of objective functions, and a combined objective function may well enhance the difficulty of searching for a global optimization solution and the complexity of minimum response surface domains. A hybrid method of PSO and VEGA was adopted to solve the inverse estimation. The standard deviation (σ) of the observed data of θ , v , or Q dividing the root mean squared error (RMSE) was called the objective function:

$$\psi = RMSE/\sigma = \sqrt{\frac{1}{m-1} \sum_{i=1}^m (Y(t_i, \beta) - Y^*(t_i))^2} \sqrt{\frac{1}{m-1} \sum_{i=1}^m (Y^*(t_i) - \bar{Y}^*(t_i))^2} \quad (9)$$

where m is the number of measurement sets (θ , v , and Q); β is the vector of optimized parameters (K_s , n , and α); Y is the corresponding model prediction data under the parameter vector β ; Y^* is the specific type of measurement data at time t_i .

The hybrid optimal VEGA-PSO algorithm presents a highly effective optimization method. Holland [39] developed a global stochastic search technique called the genetic algorithm (GA). Eberhart and Kennedy [40] developed PSO, an evolutionary optimization algorithm from the research on bird foraging behavior. In this study, multiple objectives are still present in the inverse problems of real soil hydraulic parameters, including infiltration rate (v), soil water content (θ), and cumulative infiltration (Q). The main problem in multi-objective optimization is that inverting a single objective tends to cause unacceptable outcomes for other objectives as the objectives conflict with each other. It is often difficult to select weights precisely and accurately for the objectives in many practical problems, even for a researcher familiar with the problem domain. Compared to a single-objective GA, VEGA provides a straightforward and efficient way for solving multi-objective problems. More details about the hybrid optimal algorithm for inverse parameters may be found in our previous paper [32].

The above-mentioned analysis focused on the parameters of K_s , n , α , and θ_s , with θ_r as its true value. The response surface of different parameter planes (K_s - θ_s , α - θ_s , n - θ_s , n - K_s , α - K_s , and α - n) was calculated for four types of soil (clay, silt, loam, and sand) with three initial soil water content levels (20, 40, and 60% effective saturation), to analyze the interaction in the objective function ψ of K_s , n , α , and θ_s . Each parameter domain was equally classified into 50 discrete points, and each response surface yielded 2500 (50×50) grid points. All operations were performed in a Windows 7 Ultimate environment using 32 GB of RAM and an Intel® XEON® CPU E5-2683 2.00 GHz processor. A 28-core server was used for computing through the algorithm.

3.2. Numerical and Laboratory Experiment Methods

3.2.1. Numerical Experiment

The SWMS-2D software [33] was used to generate infiltration data in this study. For the time-variable supply pressure head, h_0 (2 cm), the first 3 h (180 min) of the infiltration process were only taken into account. We concentrated on four soils: clay, silt, loam, and sand, with three θ_{initial} , (represented by 20, 40, and 60% effective saturation) for the inverse modeling. The initial h_i was calculated from each soil type's corresponding parameters, as shown in Table 1.

3.2.2. Laboratory Experiment

Experimental soil samples from depths of 0–60 cm were obtained from the Key Laboratory of Agricultural Soil and Water Engineering in Arid and Semiarid Areas of China (34°17'0" N and 108°04'0" E). Based on the USDA Soil Taxonomy System, soil samples were clay loam with particle size distributions of 27.30% 0–0.002 mm, 42.53% 0.002–0.020 mm, and 30.17% 0.02–2.00 mm. The experimental soils were air-dried, followed by screening through a mesh of 2 mm. Subsequently, they were compressed into a soil bin at a bulk

density of 1.30 or 1.35 g cm⁻³ to simulate in situ bulk density. Water was mixed with the soil to achieve the desired experimental soil water conductivity (SWC) values of 10, 20, and 30% for the respective bulk density before the soil was compacted into the bin. A homogeneous soil profile was then created by loading and compacting the soil into the bin at a layer of 5 cm. The experiment was designed to determine the irrigation volume. In this way, a Mariotte bottle was placed to maintain an infiltration depth of 3 cm (Figure 3). Cumulative infiltration was recorded for each minute of infiltration. Eventually, soil samples were gathered from side holes, and SWC was determined by recording the weight loss of samples after 24 h of oven drying at 105 °C.

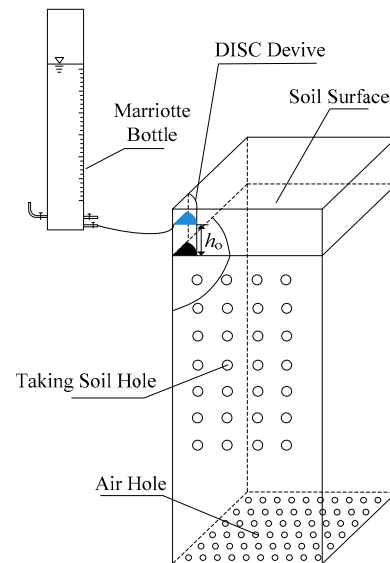


Figure 3. Simplified experimental setup (h_0 is the irrigation depth).

3.3. Evaluation Criteria

To evaluate the similarity of the inverted and real SWRCs and SWCCs, a number of points (i.e., 50) were selected on the inverted and real curves. For SWRCs, points with the same suction were selected; for SWCCs, points with the same conductivity were selected. Afterwards, the soil water content levels were calculated at each point. The statistical indices of the Nash–Sutcliffe coefficient (NS), percent bias (PBIAS), RMSE, and mean absolute error (MAE) were used to quantify the similarity between the inverted and real SWRCs and SWCCs, which are defined as follows:

$$\text{MAE} = \frac{1}{m} \sum_{i=1}^m \left| \theta_i^{\text{inv}} - \theta_i^{\text{real}} \right|, \quad (10)$$

$$\text{RMSE} = \sqrt{\frac{1}{m-1} \sum_{i=1}^m (\theta_i^{\text{inv}} - \theta_i^{\text{real}})^2}, \text{ for } i = 1, 2, \dots, n, \quad (11)$$

$$\text{PBIAS} = \frac{\sum_{i=1}^m (\theta_i^{\text{inv}} - \theta_i^{\text{real}})}{\sum_{i=1}^m \theta_i^{\text{real}}}, \quad (12)$$

$$\text{NS} = 1 - \frac{\sum_{i=1}^m (\theta_i^{\text{inv}} - \theta_i^{\text{real}})^2}{\sum_{i=1}^m (\theta_i^{\text{real}} - \overline{\theta_i^{\text{real}}})^2} \quad (13)$$

where θ_i^{real} is the i th point of the soil water content of the real SWRCs and SWCCs, with the same conductivity and suction; θ_i^{inv} is the i th point of the soil water content of the inverted SWRCs and SWCCs; m is the number (50) of selected points in the inverted and real SWRCs and SWCCs.

4. Results and Discussion

4.1. Response Surface and Uniqueness

The objective function surfaces of 12 typical soils had similar shapes (Table 1). Therefore, only the response surface of loam with 40% initial soil water content was shown in this paper. Figure 4 presents the response surface of parameter planes α - n (a), α - K_s (b), n - K_s (c), n - θ_s (d), α - θ_s (e), and K_s - θ_s (f), with the remaining two parameters as the real values, which were determined using the objective function $\psi(\theta_{\text{final}})$. Clear visual observation was facilitated by selecting logarithmic coordinates for K_s and α .

Figure 4a shows a surface with a wide valley resulting from high n and low α , whereas Figure 4b,c show narrow and long valleys for α - K_s and n - K_s . As can be observed from the first three valley contours in Figure 4a–c, it remains difficult to determine the optimal stability values of K_s , n , and α from $\psi(\theta_{\text{final}})$ even though the other two parameters are identified. In Figure 4d–f, however, smooth uniform rings with distinct extreme values in each minimum circle were shown on all three response surfaces (θ_s - K_s , θ_s - α , and θ_s - n), suggesting that the true value of θ_s may be obtained using the objective function $\psi(\theta_{\text{final}})$.

The feasibility of applying $\psi(Q)$ and $\psi(v)$ as the objective functions to inverse the remaining parameters (K_s , n , and α) through the response surface was then analyzed based on the present method. The results are shown in Figures 5 and 6. It can be seen from Figure 5a–c that the response surfaces corresponding to α - n , α - K_s , and n - K_s have obvious global optimal characteristics, indicating that it is possible to invert α , n , and K_s according to the objective function of $\psi(v)$ after θ_s is determined. Furthermore, the regions where the optimized results (α , n and K_s) are close to the true values in each response surface (Figure 5a–c) are enlarged, as indicated in Figure 5d–f. It can be seen from Figure 5e, f that there are obvious global optimal solutions in response surfaces of n - K_s and α - n . However, the response surfaces show some bubbles in the global optimal solution area, which indicates that the optimal solutions are not unique. Thus, it is demonstrated that the solutions are non-unique if only $\psi(v)$ is applied as the objective function to inverse α , n , and K_s simultaneously.

Moreover, taking $\psi(Q)$ as the objective function, Figure 6a–c illustrates that the optimal solutions of n - K_s , α - K_s , and α - n response surfaces are narrow and long regions, which are relatively small compared to Figure 4a–c. Meanwhile, the above similar approach is adopted to enlarge the regions where the inversion results of α , n , and K_s are close to the true values in each response surface (Figure 6a–c). It is further proved that the optimal solution range of the response surfaces of n - K_s , α - K_s , and α - n is smaller with $\psi(Q)$ as the objective function, as shown in Figure 6d–f.

In summary, with the $\psi(\theta_{\text{final}})$ as the objective function, the genetic algorithm (GA) is applied to inverse θ_s ; if $\psi(v)$ or $\psi(Q)$ is used as the objective function separately, the response surface of α - n (Figure 5e), n - K_s (Figure 5f), and α - K_s (Figure 6d) shows that synchronous inversion of α , n , and K_s is feasible, but the solutions are not unique. However, the stability of the inversion results can be improved if both $\psi(v)$ and $\psi(Q)$ are used as the objective functions simultaneously. The detailed objective function and solution method used in the inversion process of soil hydraulic characteristic parameters are the same as our previous paper (Yi-bo Li et al., 2018).

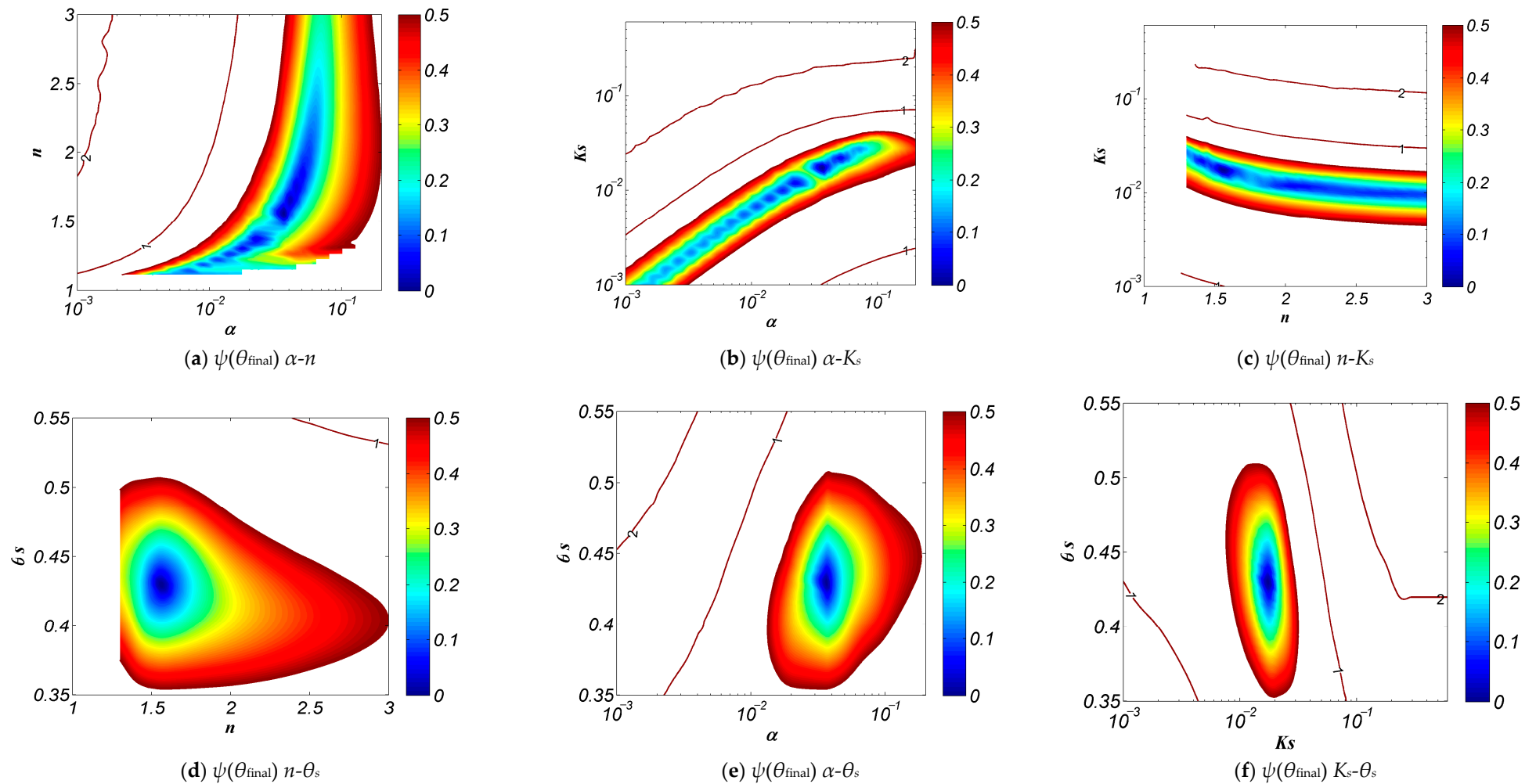


Figure 4. Contours of the objective function $\psi(\theta_{\text{final}})$ of loam with θ_{initial} as 40% effective saturation. The hydraulic parameters of loam: $K_s = 0.0173 \text{ cm}\cdot\text{min}^{-1}$; $n = 1.56$; $\alpha = 0.036 \text{ cm}^{-1}$; $\theta_s = 0.43 \text{ cm}^3\cdot\text{cm}^{-3}$; $\theta_r = 0.078 \text{ cm}^3\cdot\text{cm}^{-3}$. Results are plotted in the parameter planes of (a) α - n , (b) α - K_s , (c) n - K_s , (d) n - θ_s , (e) α - θ_s , and (f) K_s - θ_s .

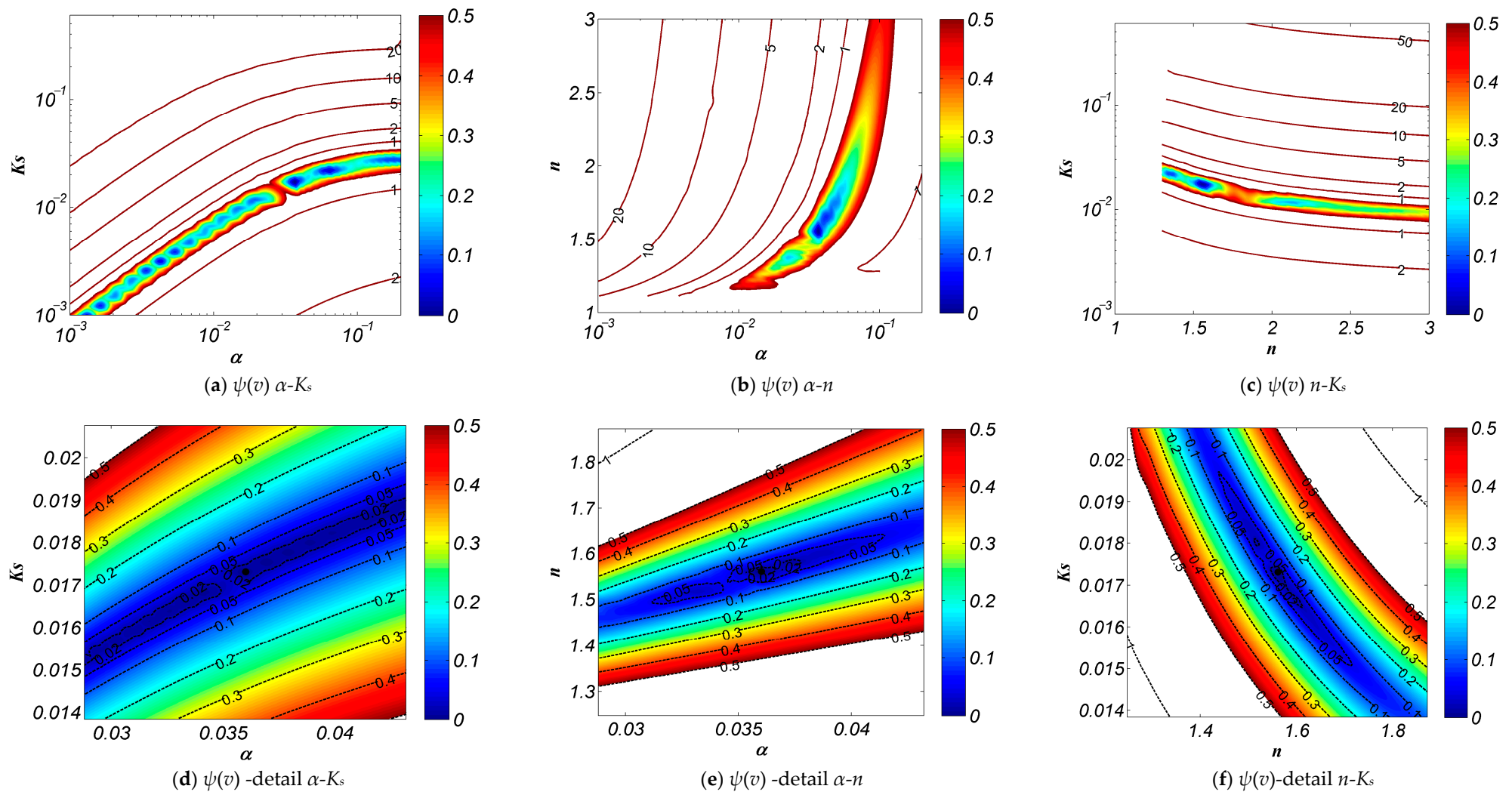


Figure 5. Contours of the objective function $\psi(v)$ of loam with θ_{initial} as 40% effective saturation. The hydraulic parameters of loam: $K_s = 0.0173 \text{ cm} \cdot \text{min}^{-1}$; $n = 1.56$; $\alpha = 0.036 \text{ cm}^{-1}$; $\theta_s = 0.43 \text{ cm}^3 \cdot \text{cm}^{-3}$; $\theta_r = 0.078 \text{ cm}^3 \cdot \text{cm}^{-3}$. Results are plotted in the parameter planes of (a,d) α - K_s , (b,e) α - n , and (c,f) n - K_s . The global scale is depicted in (a–c), while the local scale near the minimum is depicted in (d–f).

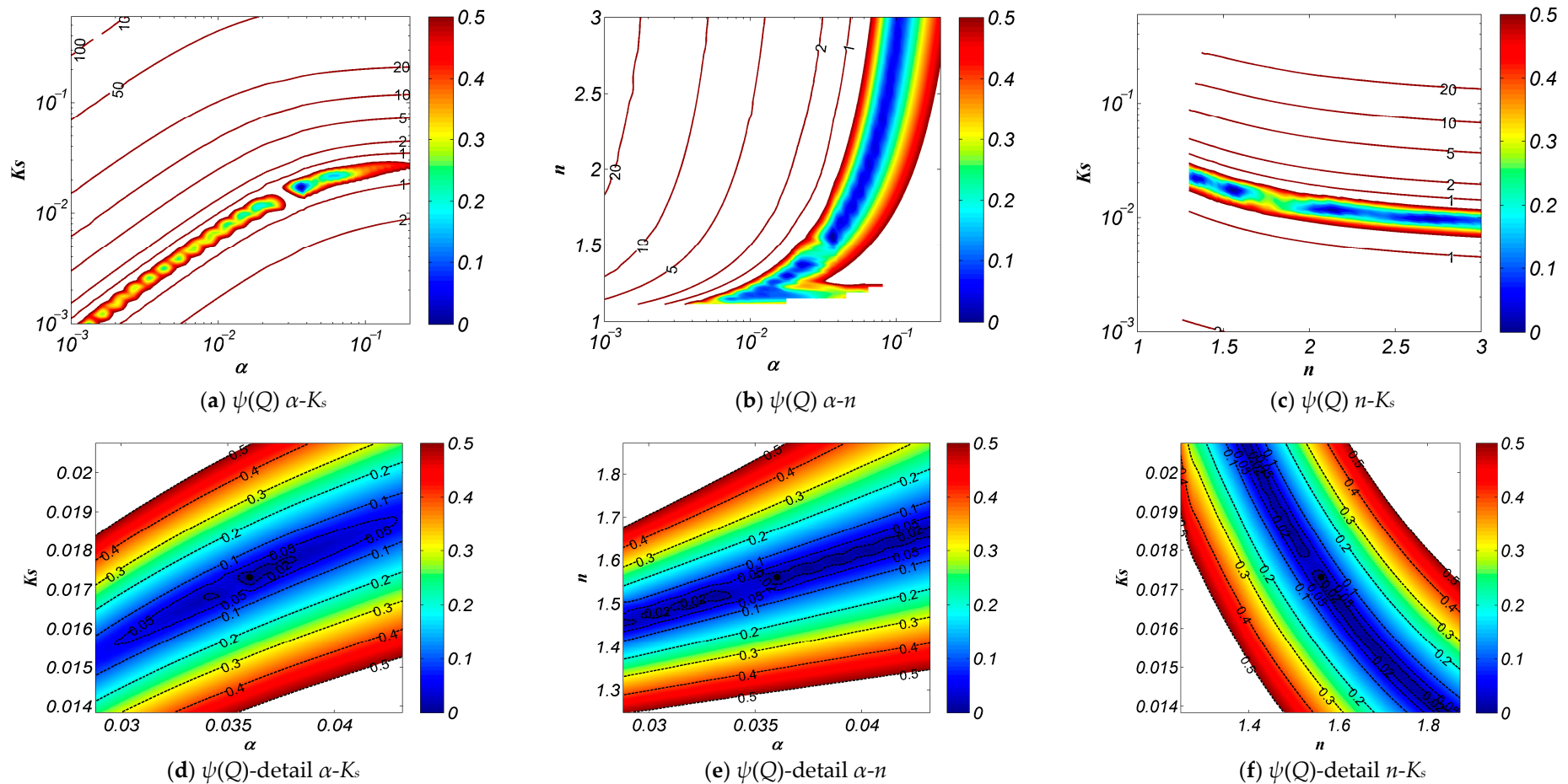


Figure 6. Contours of the objective function $\psi(Q)$ of loam with θ_{initial} as 40% effective saturation. The hydraulic parameters of loam: $K_s = 0.0173 \text{ cm} \cdot \text{min}^{-1}$; $n = 1.56$; $\alpha = 0.036 \text{ cm}^{-1}$; $\theta_s = 0.43 \text{ cm}^3 \cdot \text{cm}^{-3}$; $\theta_r = 0.078 \text{ cm}^3 \cdot \text{cm}^{-3}$. Results are plotted in the parameter planes of (a,d) α - K_s , (b,e) α - n , and (c,f) n - K_s . The global scale is depicted in (a–c), while the local scale near the minimum is depicted in (d–f).

4.2. Inverse Solution and Analysis of the Numerical Experiment

4.2.1. Inverse Solutions

A total of 12 case studies were conducted using four typical RETC soils (clay, silt, loam, and sand) with three initial water content levels, to validate the feasibility of the method. The 12 case results of the parameter inversion are summarized in Table 3, indicating that the inverted and real values were similar for each parameter.

Table 3. Inverted parameters of four typical soils with three initial water content levels.

Category		θ_r	θ_s	α	n	K_s
		$\text{cm}^3 \cdot \text{cm}^{-3}$	$\text{cm}^3 \cdot \text{cm}^{-3}$	cm^{-1}	-	$\text{cm} \cdot \text{min}^{-1}$
Sand	20%		0.4296	0.1654	2.7732	0.5005
	40%	0.0450	0.4296	0.1421	2.8061	0.4911
	60%		0.4331	0.1546	2.8622	0.5024
	Real Value	0.0450	0.4300	0.1450	2.6800	0.4950
Loam	20%		0.4296	0.0426	1.7440	0.0162
	40%	0.0780	0.4319	0.0373	1.5798	0.0176
	60%		0.4284	0.0610	1.7601	0.0187
	Real Value	0.0780	0.4300	0.0360	1.5600	0.0173
Silt	20%		0.4568	0.0202	1.3790	0.0050
	40%	0.0340	0.4567	0.0190	1.3758	0.0047
	60%		0.4611	0.0150	1.3684	0.0037
	Real Value	0.0340	0.4600	0.0160	1.3700	0.0042
Clay	20%		0.3845	0.0053	1.0923	0.0022
	40%	0.0680	0.3788	0.0047	1.0919	0.0020
	60%		0.3814	0.0038	1.0805	0.0018
	Real Value	0.0680	0.3800	0.0080	1.0900	0.0033

4.2.2. Analysis of Inverse Solutions

Table 4 lists the real and inverted parameter values that were employed to draw SWRCs and SWCCs, respectively (Figure 7). SWRCs were labeled as a1, b1, c1, and d1; SWCCs were labeled as a2, b2, c2, and d2. There are small differences between the real and inverted parameter values of K_s , n , and α , however, the real and inverted SWCCs and SWRCs are the same, indicating that the inverse approach is robust and effective.

Table 4. Soil water content errors calculated from SWRCs and SWCCs for the four typical soils.

Soil	From $h(\theta)$				From $K(\theta)$			
	MAE	RMSE	PBIAS (%)	NS	MAE	RMSE	PBIAS (%)	NS
Sand	0.00152	0.00192	0.3774	0.9993	0.00501	0.00818	3.2074	0.9929
Loam	0.00086	0.00101	-0.0102	0.9998	0.01468	0.02519	-7.3756	0.9645
Silt	0.00164	0.00188	-0.3742	0.9996	0.00536	0.00800	-2.1942	0.9975
Clay	0.00083	0.00123	0.1650	0.9998	0.00830	0.01214	-3.2121	0.9935

The error evaluation metrics NS, PBIAS, RMSE, and MAE were used to estimate the difference between the inverted and real curves, in order to further assess the robustness and accuracy of the proposed inverted approach. An average of 50 points was selected from the conductivity curves, $K(\theta)$ and suction curves, $h(\theta)$, followed by a calculation of the corresponding 50 soil water content levels. The calculated error evaluation indicators are shown in Table 4. The MAE, RMSE, and PBIAS values for the SWRCs were extremely small (0.00086–0.00164 $\text{cm}^3 \cdot \text{cm}^{-3}$, 0.00101–0.00192 $\text{cm}^3 \cdot \text{cm}^{-3}$, and 0.0102–0.3774%, respectively); the values for conductivity curves were also small (0.00501–0.01468 $\text{cm}^3 \cdot \text{cm}^{-3}$, 0.00800–0.02519 $\text{cm}^3 \cdot \text{cm}^{-3}$, and 2.1942–7.3756%, respectively), and the value of NS was relatively large (approximately 1.0). These values verify that the inverted method developed in this study is applicable to the inverse modeling of soil hydraulic characteristics [41,42]. Furthermore, the values indicate that the inverse method may be used to estimate the robustness and precision of SWRCs and SWCCs.

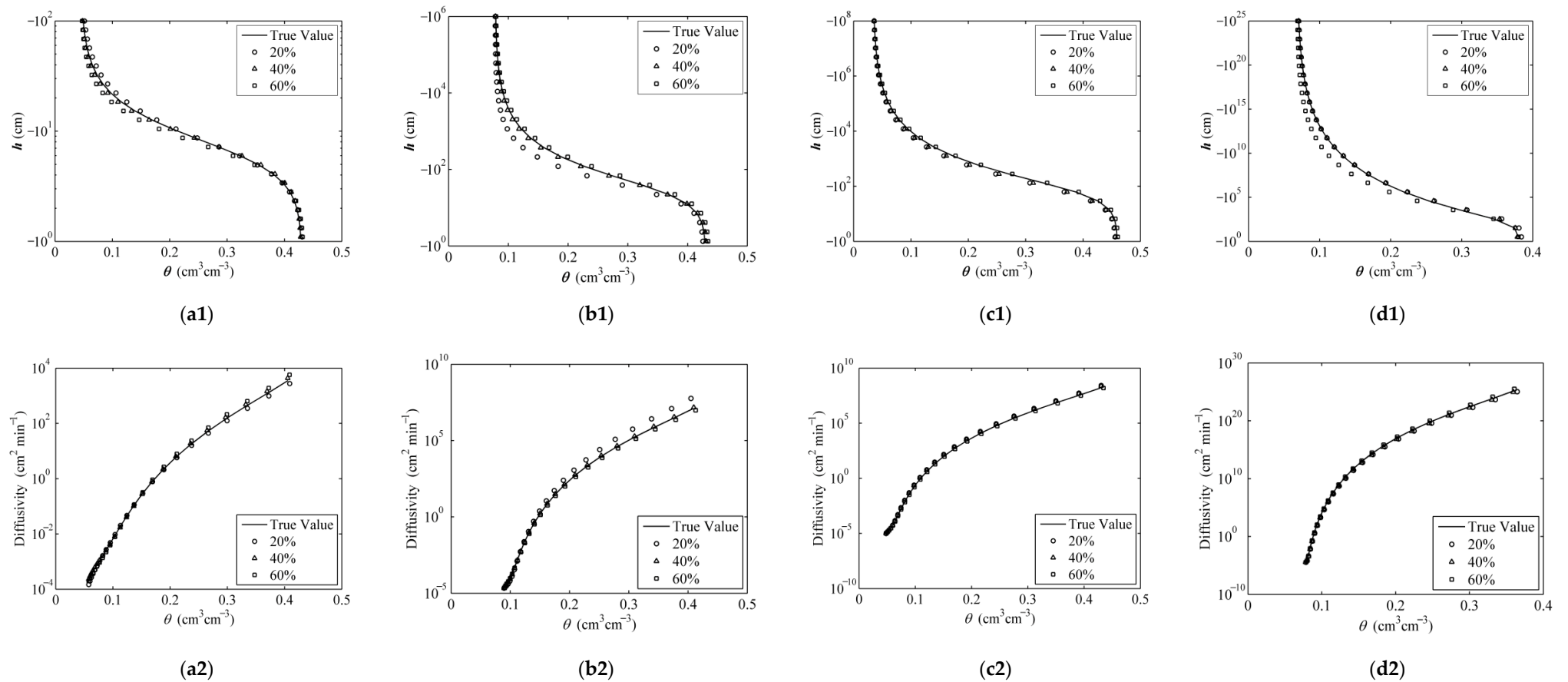


Figure 7. Comparison of soil water retention curves (a1,b1,c1,d1) and diffusivity curves (a2,b2,c2,d2) for various treatments (circle: 20% effective saturation; triangle: 40% effective saturation; square: 60% effective saturation; line: true value): (a) sand; (b) loam; (c) silt, and (d) clay. The ranges of y -axis vary depending on the different soil textures.

4.3. Inverse Solutions with Measurement Errors

There are always errors during the process of instrumentation, calibration, and other factors in practice. Hence, both the system and random errors in the initial and final water content levels, as well as the random error in the cumulative infiltration, were considered to evaluate. Table 5 shows the stability of the inverse solution. Firstly, the two system errors were set as +0.02 for θ_{initial} and -0.02 for θ_{final} , and the random error was set as 0.05 of the standard deviation (5.0%). The two random errors were then superimposed on the cumulative infiltration after being set as 0.02 and 0.05 of the standard deviation. All the inversion computations performed in the error-free inverse method were repeated for the four typical soils with θ_{initial} (40% effective saturation).

Table 5. Inverted parameters of both system and random errors in initial and final water content levels for the four typical soils.

Texture Class	Error Source	Error Category		θ_r	θ_s	α	n	K_s	
				$\text{cm}^3 \cdot \text{cm}^{-3}$	$\text{cm}^3 \cdot \text{cm}^{-3}$	cm^{-1}	-	$\text{cm} \cdot \text{min}^{-1}$	
Sand	θ_{initial}	RE	5.0%	0.0450	0.4292	0.1430	2.6512	0.4912	
		SE	$\theta_i + 0.02$ $\theta_i - 0.02$		0.4352 0.4096	0.1389 0.1281	2.6931 2.6988	0.4959 0.4912	
	θ_{final}	RE	5.0%		0.4296	0.1455	2.6780	0.4867	
		SE	$\theta_f + 0.02$ $\theta_f - 0.02$		0.4423 0.4004	0.1464 0.1449	2.6874 2.6994	0.4943 0.4877	
	Real Parameter				0.0450	0.4300	0.1450	2.6800	0.4950
	Loam	θ_{initial}	RE		5.0%	0.0780	0.4435	0.0376	1.5437
SE			$\theta_i + 0.02$ $\theta_i - 0.02$	0.4712 0.3866	0.0404 0.0341		1.5799 1.5151	0.0189 0.0191	
θ_{final}		RE	5.0%	0.4266	0.0365		1.5265	0.0188	
		SE	$\theta_f + 0.02$ $\theta_f - 0.02$	0.4798 0.3893	0.0362 0.0328		1.5761 1.5151	0.0164 0.0162	
Real Parameter			0.0780	0.4300	0.0360		1.5600	0.0173	
Silt		θ_{initial}	RE	5.0%	0.0340		0.4546	0.0159	1.3768
	SE		$\theta_i + 0.02$ $\theta_i - 0.02$	0.5035 0.4218		0.0233 0.0136	1.4474 1.2787	0.0067 0.0028	
	θ_{final}	RE	5.0%	0.4640		0.0167	1.3493	0.0046	
		SE	$\theta_f + 0.02$ $\theta_f - 0.02$	0.5072 0.4051		0.0179 0.0143	1.2825 1.2177	0.0056 0.0033	
	Real Parameter			0.0340		0.4600	0.0160	1.3700	0.0042
	Clay	θ_{initial}	RE	5.0%		0.0680	0.3965	0.0087	1.0854
SE			$\theta_i + 0.02$ $\theta_i - 0.02$	0.4241 0.3522	0.0105 0.0062		1.1220 1.0729	0.0051 0.0022	
θ_{final}		RE	5.0%	0.3774	0.0079		1.0824	0.0032	
		SE	$\theta_f + 0.02$ $\theta_f - 0.02$	0.4296 0.3514	0.0112 0.0054		1.1015 1.0681	0.0056 0.0018	
Real Parameter			0.0680	0.3800	0.0080		1.0900	0.0033	

SE = system error; RE = random error; RE 5.0% = standard deviation of random error equal to 0.05.

4.3.1. Inverse Solution Analysis Based on Initial and Final Water Content

The inverse parameter values (K_s , n , α , and θ_s) of the four typical soils are shown in Table 5. The system and random errors were superimposed on the error-free data, leading to only small deviations from the real parameters. It can be seen from Table 5 that most values of the inverse parameters were close to the real values, indicating that the approach is appropriate for practical application.

SWRCs and SWCCs were plotted to estimate the effective measurement error of the inverted value, as shown in Figures 8 and 9. The results of SWRCs and SWCCs show that the effective measurement error is still acceptable though there are small differences between the system and random error curves and the real value curves.

Table 6 displays the error evaluation metrics NS, PBIAS, and RMSE that were used to estimate the difference between the inverted results with measurement errors and the real values. An average of 50 points was selected from the conductivity curves, $K(\theta)$ and the suction curves, $h(\theta)$, followed by a calculation of the corresponding 50 soil water content levels. Table 6 presents the results of error evaluation indicators: minimal RMSEs (0.0053–0.0346 from $h(\theta)$, 0.0004–0.0216 from $K(\theta)$); small PBIASs (0.3181–14.5628 from $h(\theta)$ 0.1721–9.3637 from $K(\theta)$), and large NSs (0.9322–0.9979 from $h(\theta)$, 0.9697–1.0000 from $K(\theta)$). The results suggest that the approach is applicable to the estimation of soil hydraulic properties.

4.3.2. Inverted Solution Analysis Based on Cumulative Infiltration

Random errors only occurred during the process of cumulative infiltration; therefore, two standard deviations of 0.02 and 0.05 for random errors were analyzed in the inverted values (Table 7). Small deviations were found between the inverted values calculated from the values with measurement errors and the real values.

Figure 10 shows SWRCs and SWCCs based on the inverse values with two random errors. The inverse method is robust and reasonable for the inversion of soil hydraulic parameters, due to that, there are small differences between the inverted and real values of these curves. Table 8 details the assessment criteria NS, PBIAS, and RMSE for the inverted and real values. The robustness and effectiveness of the inverse method are represented by large NS, small PBIAS, and RMSE.

4.4. Inverse Solution and Analysis of Laboratory Experiment

4.4.1. Inverse Solution Based on Experimental Infiltration Data

Comparisons of parameter estimation results for the sandy loam are depicted in Table 9. Two $h(\theta)$ curves and $K(\theta)$ curves with hydraulic parameters inverted from the laboratory experiments are presented in Figure 11a1,a2,b1,b2, respectively. Figure 11a,b represent the results of two bulk densities (1.30 and 1.35 g cm⁻³) with three initial soil water contents. The three soft dotted lines (circle—18.92%, triangle—26.17%, and square—31.74%) were determined separately by using the VEGA-PSO inverse method, and the solid line was then determined from all three datasets from the laboratory experiments and using the same inverse method. Figure 11 illustrates that despite the small differences between the three sets of parameter values and the solid lines, they are close to each other. Table 10 displays RMSE, PBIAS, and NS for each inverse value and unified value. The robustness and effectiveness of the inverse method are represented by large NS, small PBIAS, and RMSE. Therefore, the results proved that the method proposed in this paper can be applied in laboratory experiments to invert the soil hydraulic parameters. Meanwhile, it is more intuitive to compare the two curves, $h(\theta)$ curves and $K(\theta)$ curve, to check the accuracy of the inversion than to compare the values of the individual soil hydraulic parameters individually.

4.4.2. Comprehensive Analysis of the Inverse Solution of Experimental Results

To further validate the use of the inverse solution with laboratory experimental data, the cumulative infiltration and final water content were compared between the inverse values (unified values) and the measured values. Figure 12 depicts comparisons of the cumulative infiltration for bulk densities of 1.30 and 1.35 g cm⁻³. Small deviations can be seen among the six graphs, which may be due to errors in the experiments. Figure 13 shows the distribution of final water content in the six experiments.

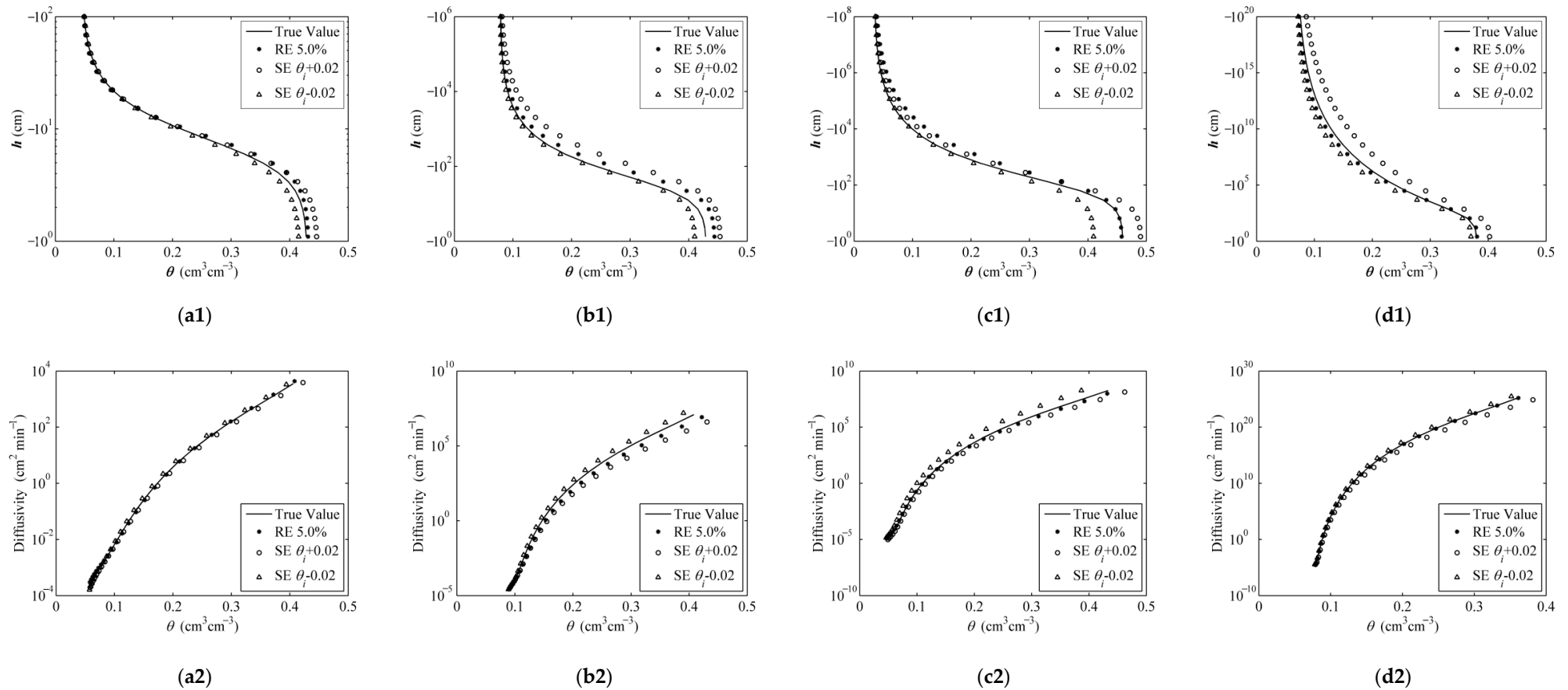


Figure 8. Comparison of SWRCs (a1,b1,c1,d1) and diffusivity curves (a2,b2,c2,d2) with system and random errors for different treatments and calculation using the objective function $f(\theta_{\text{initial}})$ (circle: 5.0% random error; triangle: 2.0% system error; square: -2.0% system error; line: true value): (a) sand; (b) loam; (c); silt, and (d) clay.

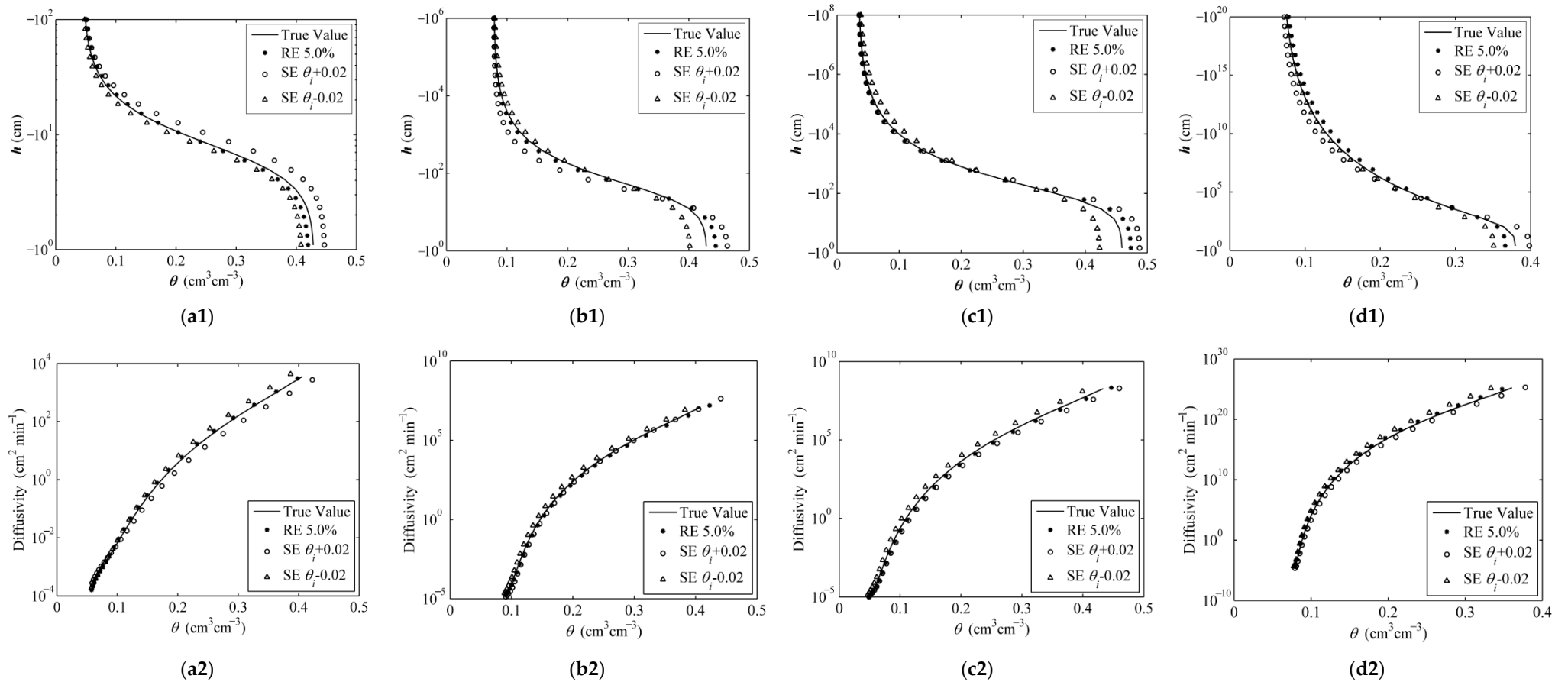


Figure 9. Comparison of SWRCs (a1, b1, c1, d1) and diffusivity curves (a2, b2, c2, d2) with system and random errors for different treatments and calculation using the objective function $f(\theta_{\text{final}})$ (circle: 5.0% random error; triangle: 2.0% system error; square: -2.0% system error; line: true value): (a) sand; (b) loam; (c); silt; (d), and clay.

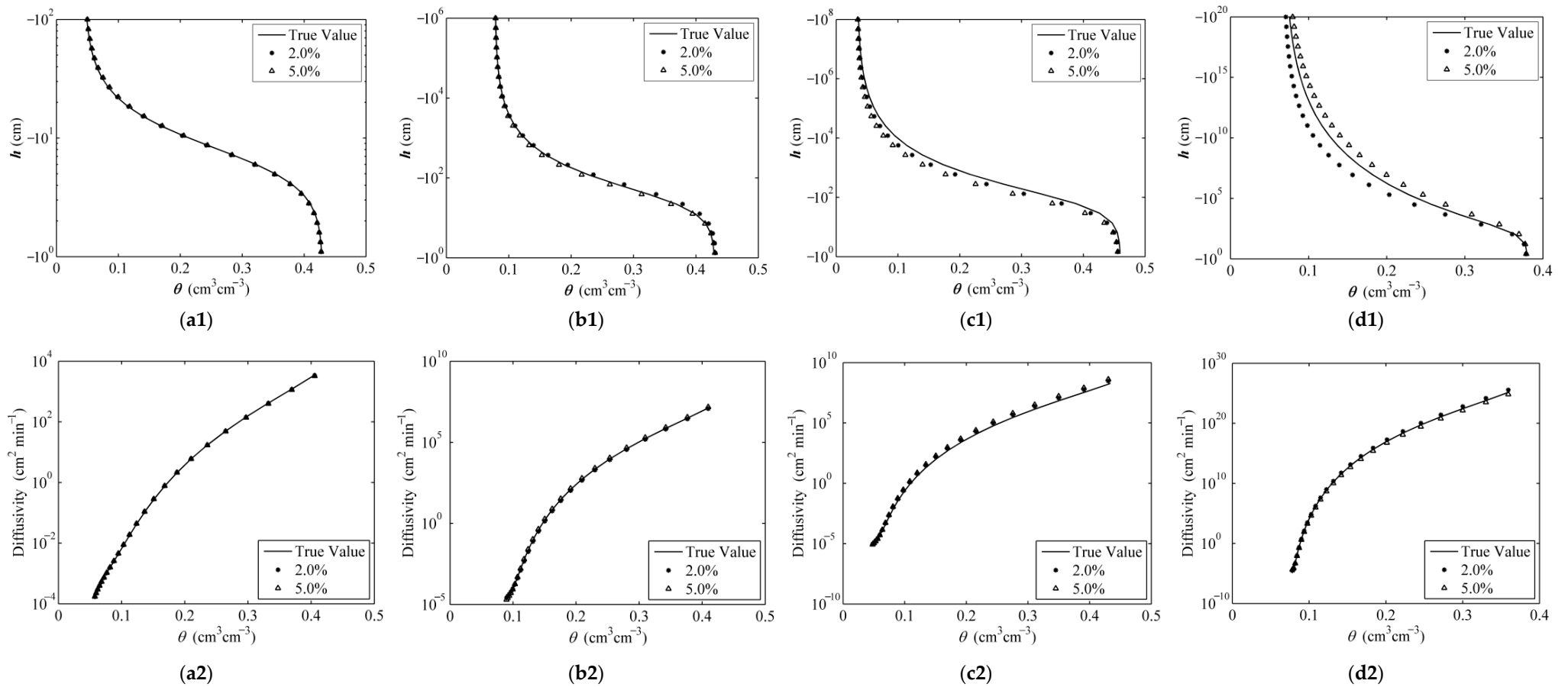


Figure 10. Comparison of SWRCs (a1,b1,c1,d1) and diffusivity curves (a2,b2,c2,d2) with system and random errors for different treatments and calculation using the objective function $f(Q)$ (circle: 5.0% random error; triangle: 2.0% system error; square: -2.0% system error; line: true value): (a) sand; (b) loam; (c); silt, and (d) clay.

Table 6. Soil water content errors calculated from inverted SWRCs and diffusivity curves given the system and random errors in initial and final water content levels for the four typical soils.

Source	Texture Class	Error Category	From $h(\theta)$			From $K(\theta)$			
			RMSE $\text{cm}^3 \cdot \text{cm}^{-3}$	PBIAS %	NS -	RMSE $\text{cm}^3 \cdot \text{cm}^{-3}$	PBIAS %	NS -	
θ_{initial}	Sand	RE	5.0%	0.0080	1.8284	0.9972	0.0011	0.4762	0.9999
		SE	$\theta_i + 0.02$	0.0103	3.1152	0.9953	0.0077	3.3904	0.9953
			$\theta_i - 0.02$	0.0098	-3.1523	0.9958	0.0055	-2.3993	0.9976
	Loam	RE	5.0%	0.0161	6.1450	0.9855	0.0064	2.4884	0.9961
		SE	$\theta_i + 0.02$	0.0346	14.3209	0.9331	0.0105	4.0688	0.9895
			$\theta_i - 0.02$	0.0092	-3.5072	0.9953	0.0082	-3.1945	0.9935
	Silt	RE	5.0%	0.0177	7.6049	0.9878	0.0007	-0.3194	1.0000
		SE	$\theta_i + 0.02$	0.0177	7.8793	0.9880	0.0134	5.7917	0.9884
			$\theta_i - 0.02$	0.0234	-7.4628	0.9787	0.0216	-9.3637	0.9697
	Clay	RE	5.0%	0.0053	-2.3265	0.9972	0.0004	0.1721	1.0000
		SE	$\theta_i + 0.02$	0.0261	14.5628	0.9322	0.0098	4.3160	0.9884
			$\theta_i - 0.02$	0.0136	-7.3473	0.9815	0.0041	-1.8139	0.9979
θ_{final}	Sand	RE	5.0%	0.0069	-1.4174	0.9979	0.0036	-1.5807	0.9990
		SE	$\theta_i + 0.02$	0.0250	9.2426	0.9723	0.0077	3.3904	0.9953
			$\theta_i - 0.02$	0.0162	-6.2018	0.9884	0.0089	-3.9233	0.9937
	Loam	RE	5.0%	0.0071	-0.3181	0.9972	0.0068	2.6550	0.9955
		SE	$\theta_i + 0.02$	0.0220	-3.7115	0.9730	0.0152	5.9101	0.9779
			$\theta_i - 0.02$	0.0139	-1.9505	0.9892	0.0118	-4.5645	0.9868
	Silt	RE	5.0%	0.0073	0.7388	0.9979	0.0061	2.6592	0.9976
		SE	$\theta_i + 0.02$	0.0146	4.0437	0.9918	0.0122	5.3064	0.9903
			$\theta_i - 0.02$	0.0175	-1.2681	0.9882	0.0157	-6.8252	0.9839
	Clay	RE	5.0%	0.0067	1.9355	0.9956	0.0059	-2.5968	0.9958
		SE	$\theta_i + 0.02$	0.0107	-2.6996	0.9886	0.0080	3.5332	0.9922
			$\theta_i - 0.02$	0.0111	-3.8752	0.9877	0.0126	-5.5379	0.9809

SR = system error; RE = random error; RE 5.0% = standard deviation of random error equal to 0.05.

Table 7. Inverted parameters with random errors in cumulative infiltration for the four typical soils.

Texture Class	Error Category	θ_r	θ_s	α	n	K_s
		$\text{cm}^3 \cdot \text{cm}^{-3}$	$\text{cm}^3 \cdot \text{cm}^{-3}$	cm^{-1}	-	$\text{cm} \cdot \text{min}^{-1}$
Sand	2.0%	0.0450	0.4314	0.1416	2.6903	0.4930
	5.0%			0.1475	2.6988	0.4987
	Real Parameter	0.0450	0.4300	0.1450	2.6800	0.4950
Loam	2.0%	0.0780	0.4285	0.0341	1.6466	0.0144
	5.0%			0.0365	1.7919	0.0124
	Real Parameter	0.0780	0.4300	0.0360	1.5600	0.0173
Silt	2.0%	0.0340	0.4623	0.0147	1.2996	0.0043
	5.0%			0.0160	1.3817	0.0039
	Real Parameter	0.0340	0.4600	0.0160	1.3700	0.0042
Clay	2.0%	0.0680	0.3812	0.0104	1.0862	0.0046
	5.0%			0.0074	1.0901	0.0027
	Real Parameter	0.0680	0.3800	0.0080	1.0900	0.0033

2.0 and 5.0% = standard deviation of random error equal to 0.02 and 0.05, respectively.

Table 8. Soil water content errors calculated from inverted SWRCs and conductivity curves with random errors in cumulative infiltration for the four typical soils.

Texture Class	Error Category	From $h(\theta)$			From $K(\theta)$		
		RMSE $\text{cm}^3 \cdot \text{cm}^{-3}$	PBIAS %	NS -	RMSE $\text{cm}^3 \cdot \text{cm}^{-3}$	PBIAS %	NS -
Sand	2.0%	0.0024	0.9524	0.9997	0.0007	0.2774	0.9997
	5.0%	0.0017	-0.4835	0.9999	0.0007	0.2774	0.9999
Loam	2.0%	0.0073	-2.6803	0.9970	0.0007	-0.2678	1.0000
	5.0%	0.0205	-7.2361	0.9765	0.0007	-0.2678	1.0000
Silt	2.0%	0.0212	9.5425	0.9826	0.0011	0.4451	0.9999
	5.0%	0.0023	-0.6324	0.9998	0.0011	0.4451	0.9999
Clay	2.0%	0.0022	0.9520	0.9995	0.0006	0.2432	1.0000
	5.0%	0.0011	0.4907	0.9999	0.0006	0.2432	1.0000

2.0 and 5.0% = standard deviation of random error equal to 0.02 and 0.05, respectively.

Table 9. Inverse solution results for the sandy loam in laboratory experiments.

Bulk Density	Category	θ_r $\text{cm}^3 \cdot \text{cm}^{-3}$	θ_s $\text{cm}^3 \cdot \text{cm}^{-3}$	α cm^{-1}	n -	K_s $\text{cm} \cdot \text{min}^{-1}$
1.30	18.92%		0.48354	0.00810	1.59852	0.01314
	26.17%	0.0785	0.47984	0.00789	1.78034	0.01131
	31.74%		0.48102	0.00668	1.84100	0.01157
	Unified Value	0.0785	0.4830	0.0074	1.6785	0.0124
1.35	18.92%		0.51158	0.00659	1.89324	0.01200
	26.17%	0.0730	0.49996	0.00660	1.66160	0.01195
	31.74%		0.50281	0.00610	1.86946	0.01323
	Unified Value	0.0730	0.5020	0.0062	1.8126	0.0129

Table 10. Error analyses for three initial water content levels.

Bulk Density	Initial Water Content	From $h(\theta)$			From $K(\theta)$		
		RMSE $\text{cm}^3 \cdot \text{cm}^{-3}$	PBIAS %	NS -	RMSE $\text{cm}^3 \cdot \text{cm}^{-3}$	PBIAS %	NS -
1.30	18.92%	0.0171	-4.8737	0.9899	0.0012	0.4614	0.9999
	26.17%	0.0155	-3.8097	0.9917	0.0008	-0.3145	0.9999
	31.74%	0.0057	1.3477	0.9989	0.0002	-0.0679	1.0000
1.35	18.92%	0.0187	2.7418	0.9901	0.0039	-1.3463	0.9990
	26.17%	0.0059	-0.1101	0.9990	0.0029	-1.0163	0.9994
	31.74%	0.0086	0.5048	0.9979	0.0032	1.1095	0.9993

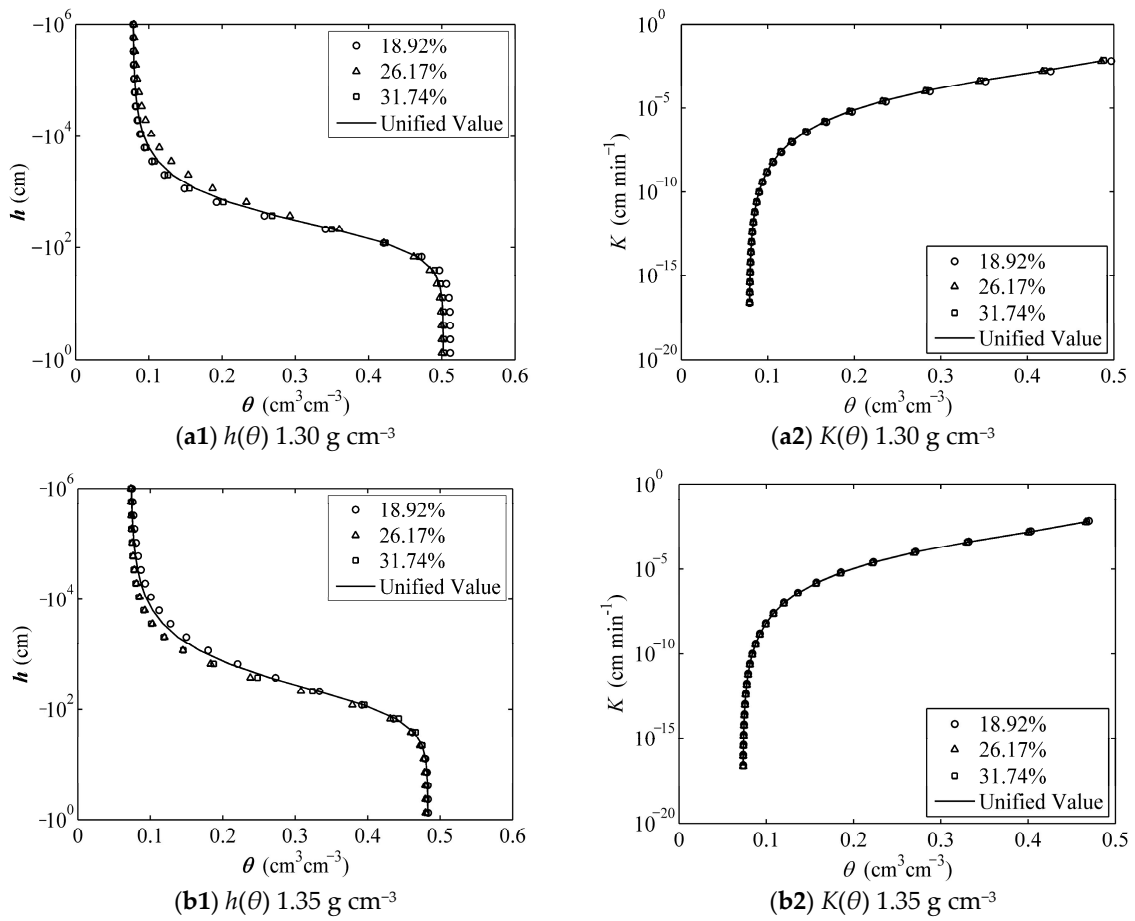


Figure 11. Comparison of soil water conductivity curves and SWRCs of the three experimental solutions.

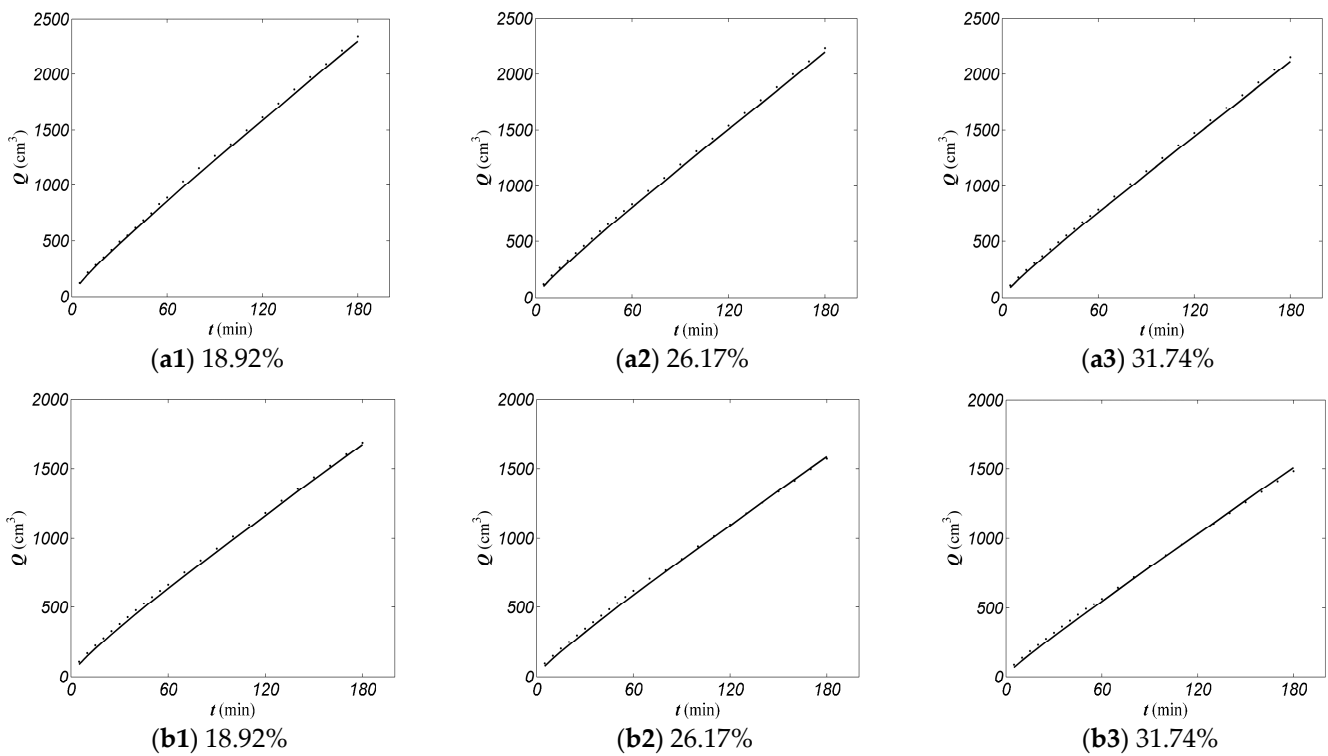


Figure 12. Comparison of cumulative infiltration for three initial water content levels.

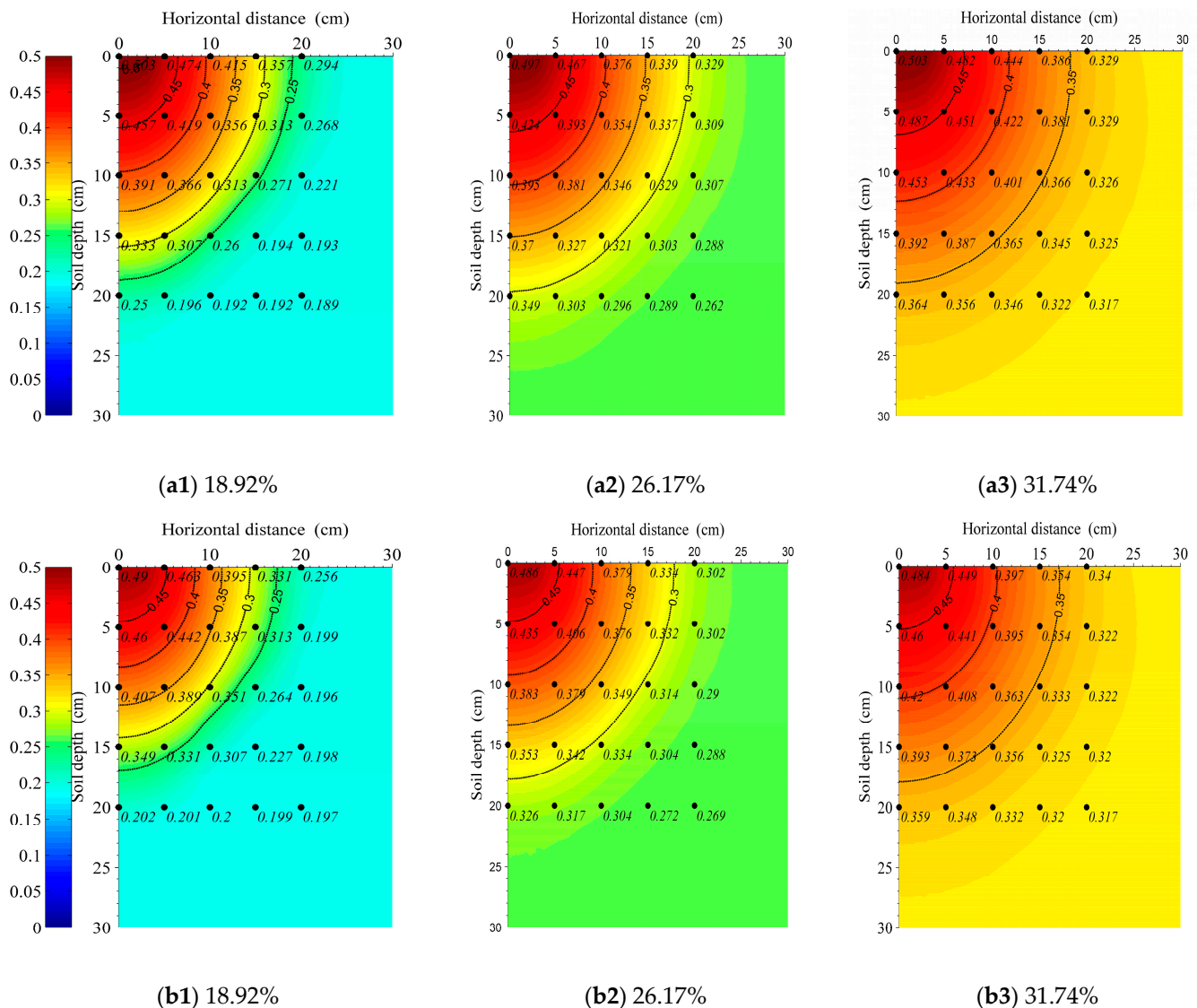


Figure 13. Comparison of final water distribution for three initial water content levels.

5. Conclusions

This study investigated the inverse determination of soil hydraulic properties based on the van Genuchten–Mualem model and data from simultaneously measured cumulative infiltration and final water content. The proposed two-step inverse estimation method was employed to compare numerically simulated values and measurements from laboratory experiments, indicating that the data were consistent. Moreover, new formulations of α/K_s and v/K_s were applied in the inverse procedure to reduce the scope of K_s , increasing the efficiency of the method. After the inverse procedure was performed, the GA with θ_{final} was used to determine the saturated water content θ_s . Finally, the soil characteristic parameters K_s , n , and α were accurately inverted by using the VEGA-PSO-based multi-objective optimization method according to the infiltration rate, final water content, and cumulative infiltration.

In terms of validating the accuracy of the model, no separate comparison of the values of each soil hydraulic parameter was made, while considering that the parameters previously influenced each other, and two curves $h(\theta)$ and $K(\theta)$ were plotted for accuracy analysis. Additionally, the model was verified in the case of measurement errors (system error and random error) that exist in the practical situation.

The general agreement between the numerical simulations and inverse solutions for $h(\theta)$ and $K(\theta)$ suggested that the proposed inverse method is very effective. The results obtained directly from laboratory experiments were also found to agree with the inverse solutions. The robustness and practicability of the proposed method were validated given that the accuracy of results was acceptable. However, further investigation is required for the inhomogeneity of soil water content distribution and soil texture. Moreover, the estimation of soil hydraulic parameters on field plot and large spatial scale needs more thorough research. Li, Y.-B.; Liu, Y.; Ma, X.-Y.

Author Contributions: Conceptualization, X.M. and Y.L. (Yibo Li); methodology, Y.L. (Yibo Li); software, Y.L. (Ye Liu); validation, Y.L. (Yibo Li) and Y.L. (Ye Liu); formal analysis, Y.L. (Yibo Li); investigation, Y.L. (Yibo Li); resources, Y.L. (Yibo Li); data curation, Y.L. (Yibo Li) and Y.L. (Ye Liu); writing—original draft preparation, Y.L. (Yibo Li); writing—review and editing, X.M.; visualization, Y.L. (Yibo Li) and Y.L. (Ye Liu); supervision, X.M.; project administration, X.M.; funding acquisition, X.M. and Y.L. (Yibo Li). All authors have read and agreed to the published version of the manuscript.

Funding: This research was funded by the Projects of the National Natural Science Foundation of China (No. 51909208) and the Postdoctoral Science Foundation of China (2019M663789).

Data Availability Statement: Not applicable.

Conflicts of Interest: The authors declare no conflict of interest.

References

- Russo, D.; Bresler, E. Soil Hydraulic Properties as Stochastic Processes: I. An Analysis of Field Spatial Variability. *Soil Sci. Soc. Am. J.* **1981**, *45*, 682–687. [\[CrossRef\]](#)
- Chen, P.-Y.; Chen, C.-H.; Hsu, N.-S.; Wu, C.-M.; Wen, J.-C. Influence of heterogeneity on unsaturated hydraulic properties: (1) local heterogeneity and scale effect. *Hydrol. Process.* **2012**, *26*, 3593–3603. [\[CrossRef\]](#)
- van Genuchten, M.T.; Šimůnek, J. *Evaluation of Pollutant Transport in the Unsaturated Zone, Regional Approaches to Water Pollution in the Environment*; Springer: Dordrecht, The Netherlands, 1996.
- Green, R.E.; Ahuja, L.R.; Chong, S.K.; Klute, A. Hydraulic conductivity, diffusivity, and sorptivity of unsaturated soils: Field methods. In *Methods of Soil Analysis: Part 1 Physical and Mineralogical Methods, 5.1*, 2nd ed.; American Society of Agronomy: Washington, DC, USA, 1986; pp. 771–798.
- Klute, A.; Dirksen, C. Hydraulic conductivity of saturated soils: Field methods. *Methods Soil Anal.* **1986**, *5*, 687–734.
- Baroni, G.; Facchi, A.; Gandolfi, C.; Ortuani, B.; Horeschi, D.; van Dam, J.C. Uncertainty in the determination of soil hydraulic parameters and its influence on the performance of two hydrological models of different complexity. *Hydrol. Earth Syst. Sci.* **2010**, *14*, 251–270. [\[CrossRef\]](#)
- Vrugt, J.A.; Stauffer, P.H.; Wöhling, T.; Robinson, B.A.; Vesselinov, V.V. Inverse Modeling of Subsurface Flow and Transport Properties: A Review with New Developments. *Vadose Zone J.* **2008**, *7*, 843–864. [\[CrossRef\]](#)
- Hopmans, J.W.; Šimůnek, J. Review of inverse estimation of soil hydraulic properties. p. 643–659. In *Characterization and Measurement of the Hydraulic Properties of Unsaturated Porous Media*; U.S. Salinity Laboratory: Riverside, CA, USA, 1999.
- Hopmans, J.W.; Šimůnek, J.; Romano, N.; Durner, W. Simultaneous determination of water transmission and retention properties: Inverse methods. In *Methods of Soil Analysis. Part 4. Physical Methods*; Dane, J., Topp, G., Eds.; SSSA Book Series 5; SSSA: Madison, WI, USA, 2002; pp. 963–1008.
- Wang, C.-N.; Yang, F.-C.; Nguyen, V.T.T.; Vo, N.T.M. CFD Analysis and Optimum Design for a Centrifugal Pump Using an Effectively Artificial Intelligent Algorithm. *Micromachines* **2022**, *13*, 1208. [\[CrossRef\]](#)
- Huynh, N.T.; Nguyen, T.V.T.; Nguyen, Q.M. Optimum Design for the Magnification Mechanisms Employing Fuzzy Logic–ANFIS. *Comput. Mater. Contin.* **2022**, *73*, 5961–5983. [\[CrossRef\]](#)
- Kuznetsova, A.; Maleva, T.; Soloviev, V. Using YOLOv3 Algorithm with Pre- and Post-Processing for Apple Detection in Fruit-Harvesting Robot. *Agronomy* **2020**, *10*, 1016. [\[CrossRef\]](#)
- Katsaggelos, A.; Lay, K. Maximum likelihood blur identification and image restoration using the EM algorithm. *IEEE Trans. Signal Process.* **1991**, *39*, 729–733. [\[CrossRef\]](#)
- Taghizadeh-Mehrjardi, R.; Nabiollahi, K.; Rasoli, L.; Kerry, R.; Scholten, T. Land Suitability Assessment and Agricultural Production Sustainability Using Machine Learning Models. *Agronomy* **2020**, *10*, 573. [\[CrossRef\]](#)
- Kavakiotis, I.; Tsave, O.; Salifoglou, A.; Maglaveras, N.; Vlahavas, I.; Chouvarda, I. Machine Learning and Data Mining Methods in Diabetes Research. *Comput. Struct. Biotechnol. J.* **2017**, *15*, 104–116. [\[CrossRef\]](#) [\[PubMed\]](#)
- Hoefer, M.J.D. Automated Design for Manufacturing and Supply Chain Using Geometric Data Mining and Machine Learning. Master's Thesis, Iowa State University, Ames, IA, USA, 2017.
- Kool, J.; Parker, J.; van Genuchten, M. Parameter estimation for unsaturated flow and transport models—A review. *J. Hydrol.* **1987**, *91*, 255–293. [\[CrossRef\]](#)

18. van Genuchten, M.T. *Non-Equilibrium Transport Parameters from Miscible Displacement Experiments*; US Salinity Laboratory, US Department of Agricultural Research: Riverside, CA, USA, 1981.
19. Parker, J.C.; Van Genuchten, M.T. Determining transport parameters from laboratory and field tracer experiments. *Bull. Va. Agric. Exp. Stn.* **1984**, *84*-3, 96.
20. Dane, J.H.; Hruska, S. In-Situ Determination of Soil Hydraulic Properties during Drainage. *Soil Sci. Soc. Am. J.* **1983**, *47*, 619–624. [[CrossRef](#)]
21. Zachmann, D.W.; Duchateau, P.; Klute, A. The Calibration of the Richards Flow Equation for a Draining Column by Parameter Identification. *Soil Sci. Soc. Am. J.* **1981**, *45*, 1012–1015. [[CrossRef](#)]
22. Parker, J.C.; Kool, J.B.; van Genuchten, M.T. Determining soil hydraulic properties from one-step outflow experiments by parameter estimation, II, Experimental studies. *Soil Sci. Soc. Am. J.* **1985**, *49*, 1354–1359. [[CrossRef](#)]
23. Kool, J.B.; Parker, J.C.; van Genuchten, M.T. ONESTEP: A nonlinear parameter estimation program for evaluating soil hydraulic properties from one-step outflow experiments. *Bull. Va. Agric. Exp. Stn.* **1985**.
24. Kool, J.B.; Parker, J.C.; van Genuchten, M.T. Determining soil hydraulic properties from one-step outflow experiments by parameter estimation, I, Theory and numerical studies. *Soil Sci. Soc. Am. J.* **1985**, *49*, 1348–1354. [[CrossRef](#)]
25. Eching, S.O.; Hopmans, J.W. Optimization of Hydraulic Functions from Transient Outflow and Soil Water Pressure Data. *Soil Sci. Soc. Am. J.* **1993**, *57*, 1167–1175. [[CrossRef](#)]
26. van Dam, J.C.; Stricker, J.N.M.; Droogers, P. Inverse Method to Determine Soil Hydraulic Functions from Multistep Outflow Experiments. *Soil Sci. Soc. Am. J.* **1994**, *58*, 647–652. [[CrossRef](#)]
27. Russo, D.; Bresler, E.; Shani, U.; Parker, J.C. Analysis of infiltration events in relation to determining soil hydraulic properties by inverse problem methodology. *Water Resour. Res.* **1991**, *27*, 1361–1373. [[CrossRef](#)]
28. Bohne, K.; Roth, C.; Leij, F.J.; VAN Genuchten, M.T. Rapid method for estimating the unsaturated hydraulic conductivity from infiltration measurement. *Soil Sci.* **1993**, *155*, 237–244. [[CrossRef](#)]
29. Kool, J.B.; Parker, J.C. Analysis of the inverse problem for transient unsaturated flow. *Water Resour. Res.* **1988**, *24*, 817–830. [[CrossRef](#)]
30. van Dam, J.C.; Stricker, J.N.M.; Droogers, P. Inverse Method for Determining Soil Hydraulic Functions from One-Step Outflow Experiments. *Soil Sci. Soc. Am. J.* **1992**, *56*, 1042–1050. [[CrossRef](#)]
31. van Genuchten, M.V.; Leij, F.J.; Yates, S.R. *The RETC Code for Quantifying the Hydraulic Functions of Unsaturated Soils: Project Summary*; U.S. Environmental Protection Agency, Research and Development, Robert S. Kerr Environmental Research Laboratory: Ada, OK, USA, 1992.
32. Li, Y.B.; Liu, Y.; Nie, W.B.; Ma, X.Y. Inverse Modeling of Soil Hydraulic Parameters Based on a Hybrid of Vector-Evaluated Genetic Algorithm and Particle Swarm Optimization. *Water* **2018**, *10*, 84. [[CrossRef](#)]
33. Šimůnek, J.; Vogel, T.; Genuchten, M. *The SWMS-2D for Simulating Water Flow and Solute Transport in Two-Dimensional Variably Saturated Media: Version 1.21*; USDA: Riverside, CA, USA, 1994.
34. van Genuchten, M.T. A Closed-form Equation for Predicting the Hydraulic Conductivity of Unsaturated Soils. *Soil Sci. Soc. Am. J.* **1980**, *44*, 892–898. [[CrossRef](#)]
35. Ciollaro, G.; Romano, N. Spatial variability of the hydraulic properties of a volcanic soil. *Geoderma* **1995**, *65*, 263–282. [[CrossRef](#)]
36. Pham, H.Q.; Fredlund, D.G.; Barbour, S.L. A study of hysteresis models for soil-water characteristic curves. *Can. Geotech. J.* **2005**, *42*, 1548–1568. [[CrossRef](#)]
37. Xing, X.; Liu, Y.; Ma, X. A modified van-Genuchten model for soil-water retention modeling by considering plant additives. *Arch. Agron. Soil Sci.* **2018**, *65*, 435–449. [[CrossRef](#)]
38. Leij, F.J.; Alves, W.J.; Genuchten, M.T.V.; Williams, J.R. *Unsoda Unsaturated Soil Hydraulic Database*; Report EPA/600/r96/095; US Environmental Protection Agency: Ada, OK, USA, 1996; 103p.
39. Holland, J.H. *Adaptation in Natural and Artificial Systems*, 1st ed.; University of Michigan Press: Ann Arbor, MI, USA, 1975.
40. Eberhart, R.; Kennedy, J. A new optimizer using particle swarm theory. In Proceedings of the Mhs95 Sixth International Symposium on Micro Machine & Human Science IEEE, Nagoya, Japan, 4–6 October 1995.
41. Moriasi, D.N.; Arnold, J.G.; Van Liew, M.W.; Bingner, R.L.; Harmel, R.D.; Veith, T.L. Model Evaluation Guidelines for Systematic Quantification of Accuracy in Watershed Simulations. *Trans. ASABE* **2007**, *50*, 885–900. [[CrossRef](#)]
42. Xing, X.; Kang, D.; Ma, X. Differences in loam water retention and shrinkage behavior: Effects of various types and concentrations of salt ions. *Soil Tillage Res.* **2017**, *167*, 61–72. [[CrossRef](#)]

Disclaimer/Publisher’s Note: The statements, opinions and data contained in all publications are solely those of the individual author(s) and contributor(s) and not of MDPI and/or the editor(s). MDPI and/or the editor(s) disclaim responsibility for any injury to people or property resulting from any ideas, methods, instructions or products referred to in the content.